Desalination and Water Treatment
www.deswater.com

doi: 10.5004/dwt.2022.28653

266 (2022) 212–225
August

Efficient adsorption of three dyes by soybean residue (okara) biochar in an aqueous solution

Dexin Shan[a], Ziyi Shao[b], Xiao Liu[b], Yuxin Wang[b], Yufei Liu[b], Yingjie Dai[b,*]

[a]*College of Landscape Architecture and Life Science, Chongqing University of Arts and Sciences, No. 319 Honghe Road, Yongchuan District, Chongqing 402168, China, email: 410932396@qq.com (D. Shan)*
[b]*College of Resources and Environment, Northeast Agricultural University, No. 600 Changjiang Road, Xiangfang District, Harbin 150030, China, emails: 2235685992@qq.com (Z. Shao), 1812934302@qq.com (X. Liu), wyx18919653626@126.com (Y. Wang), 1253903895@qq.com (Y. Liu), dai5188@hotmail.com (Y. Dai)*

Received 8 March 2022; Accepted 10 June 2022

ABSTRACT

In this study, biochar (BC) was prepared from okara (BC-OA) and applied to the adsorption of methylene blue (MB), neutral red (NR) and malachite green (MG) in aqueous solutions. Different analytical techniques characterized the structure and surface chemical properties of the adsorbents. The results were used to analyze the adsorption interaction between BC-OA and contaminants, and a single factor test determined the optimal adsorption conditions. The results showed that the removal ratio increased with the solution pH value, indicating that the alkaline condition was more conducive to adsorption. In the adsorption–desorption regeneration experiment, the adsorption performance of BC-OA decreased slightly, reflecting the stability of BC performance. The Langmuir isothermal adsorption model could describe the adsorption process better, with correlation coefficient (R^2) of 0.9565, 0.9870 and 0.9825, and q_m of 294.04, 583.50 and 1,058.36 mg/g, respectively. The fitting results of the pseudo-first-order kinetic model show that chemisorption controls the whole adsorption process. In this work, the adsorbent (BC) was prepared by using okara biomass material. The experimental results show that the adsorption effect is good, the adsorption speed is fast, the preparation process is simple and environmentally friendly, and BC can be used as a new type of high-efficiency adsorbent, which can expand its application in dyes wastewater treatment.

Keywords: Adsorbent; Adsorption mechanism; Biochar; Dye; Effective adsorption

1. Introduction

Dyes are widely used in the paper, textile, food, leather, plastic, and pharmaceutical industries [1]. Since the beginning of the application of dye products, a large number of wastewater containing dyes or dye intermediates into the natural water body, causing water pollution of the types and quantity of dyes to continue to increase, making environmental pollution increasingly serious [2]. Dye wastewater has poor biochemical properties, high chromaticity, strong acidity and alkalinity [3]. The complex aromatic structure of dyes makes them light, heat and physicochemically stable, so it is difficult to degrade dyes, which in turn affects the normal metabolic activities of aquatic organisms and breaks the original ecological balance [4,5]. These dyes are also considered to be hazardous to human health by potentially triggering physical diseases such as allergies, hyperactivity and cancer [6]. Methylene blue (MB), neutral red (NR) and malachite green (MG) are three dyes commonly used in industry [7]. MB is a cationic thiazine dye. MB can interact with negatively charged cell membrane surfaces to enter cells, leading to bioaccumulation and biotoxicity, and the

* Corresponding author.

toxicological properties of this compound have significant effects on the metabolism of aquatic organisms, and acute exposure to MB can also cause vomiting, diarrhea, and other health disorders in humans [8]. NR is a cationic dye widely used in biological research. NR produces carbon monoxide, carbon dioxide, nitrogen oxides and hydrochlorides, which are harmful to human health [9,10]. MG is a highly toxic thiazine dye with a complex aromatic structure containing nitrogen, and its molecular structure is influenced by the pH of the solution. MG is highly genotoxic, prone to chromosome breakage, and is teratogenic and carcinogenic [11,12]. Therefore, studying the removal of these dyes from wastewater is a daunting task.

There are different methods to remove dyes from water, such as physical, biological and electrochemical [13,14]. However, these techniques are often expensive, ineffective, and time-consuming [15,16]. In this regard, adsorption is one of the most attractive technologies for removing pollutants from water and the use of biochar (BC, a solid, carbon-rich byproduct obtained from the biomass conversion process) is considered an attractive option for water purification [17–22]. BC has a large specific surface area and a good pore structure and is cheap and easy to operate, making it suitable for the adsorption of dye contamination in water. Biochar is highly organized after treatment and has a large specific surface area and good pore structure, and it is inexpensive and easy to operate [23]. With the highly porous nature of biochar, soluble organic dyes can be transferred from the wastewater to the adsorbent's surface to remove dye contamination from water [1].

Adsorption technology has been used to treat wastewater from the dye industry [21,22]. Reference studies have shown the advantages of BC from multiple biomass sources and production in dealing with environmental substrates and waste management. The maximum adsorption capacity of functionalized mesoporous magnetic BC and busulfan BC for MB was 394.3 and 121.4 mg/g, respectively [24,25]. In addition, dyes can also be removed by adsorption with other adsorbents, but the effectiveness is seen to be inferior compared to BC adsorption. The adsorption of MB using an iron-based metal–organic framework yielded an adsorption capacity of 8.65 mg/g, while the improvement of the phthalic acid metal-organic skeleton with cobalt doping could increase the adsorption capacity to 23.92 mg/g. The maximum adsorption capacity of peanut shells for NR in an aqueous solution at 22°C reached 37.5 mg/g [26–28]. However, there are few studies reported on the removal of dyes from water using BC produced from okara, so the present study is also innovative in terms of adsorbents.

In this study, BC-OA was prepared at 700°C for the adsorption of MB, NR and MG dyes. The adsorbents were characterized and determined by scanning electron microscopy, Fourier-transform infrared spectroscopy, X-ray diffraction, isoelectric point, specific surface area and pore size distribution. The effects of different factors on the adsorption effect were investigated, including reaction time, amount of adsorbent, initial concentration of dye, solution pH and solution salt ion concentration. $L_9(3^4)$ orthogonal test was designed to determine the optimal combination of experimental conditions for the three sorbents. Ads to the experimental data of the three adsorption agents using the adsorption isotherm model, kinetic model, diffusion model and thermodynamic model to explore the adsorption mechanism of dyes in water. The adsorbent was desorbed using an ultrasonic oscillator, and when the desorption was complete, it was then used to adsorb dye wastewater as a means of exploring its desorption regeneration capabilities and practical applications. This study hopes to prove that the adsorbent made of okara waste plays an important role in the recovery of dye wastewater, the establishment of a circular economy and its contribution to sustainable development.

2. Materials and methods

2.1. Materials

The bean dregs used in the experiment were from the canteen of Northeast Agricultural University. The bean dregs-based BC was carbonized at 700°C for 1 h, washed with 50 mL 5% HCl solution until the pH value was constant, washed with distilled water and dried, and the prepared adsorbent was BC-OA.

2.2. Physical and chemical properties of BC-OA

Surface microstructures such as special voids and folds were analyzed by scanning electron microscopy (SEM; Hitachi High-Tech Corporation, SU8010). The functional groups and chemical bonds were determined by infrared spectroscopy (Shimadzu Instrument Co., Ltd., Japan, 840S). The lattice space structure and mineral composition were analyzed by X-ray diffractometry (Nippon Science Company, Dmax/2200); The isoelectric point was determined by pH drift determination method (Shanghai Instrument Electrical Scientific Instrument Co., LTD., PHS-3C); N_2 adsorption method was used to determine the specific surface area and pore size distribution of BC-OA. Under the relative pressure ratio P/P_0 = 0.994, the pore size distribution is calculated by Barrett–Joyner–Halenda method and Dubinin–Radushkevich method. Besides Brunauer–Emmett–Teller (BET) method was used to estimate the specific surface area.

2.3. Adsorption experiment

Each dye (MB, NR, MG) of the standard solution was respectively 1–10 mg/L, and a blank control group in the preparation of linear calibration curve made by distilled water. In addition factor test, 25 mg/L dye MB, NR and MG solution 25 mL were taken respectively, and the addition amount of adsorbent was 0.4–1.2 g/L. For initial concentration test, respectively take 25–250 mg/L dye MB, NR and mg solution 25 mL. In the experiment on influencing factors of pH value, 0.1 mol/L hydrochloric acid and sodium hydroxide were used to adjust the pH of the solution, so that the pH range of the solution was 2.0–12.0.

Adsorption kinetics set different reaction time intervals of 0–240 min, respectively. Based on this data, relevant parameters were fitted to the pseudo-first-order kinetics model and the pseudo-second-order kinetics model. NaCl was added to explore the influence of the concentration of salt ions in the solution on the adsorption effect. The concentration of NaCl was 0–4 mol/L. In the adsorption isotherm test, take 25–600 mg/L of dye MB and Mg solution 25 mL,

and adsorption isotherms were plotted according to equilibrium concentration and adsorption capacity, and relevant parameters were obtained by fitting the Langmuir model, Freundlich model and Temkin model. Take dyes with concentrations of 25–600 mg/L respectively, and MB, NR and Mg solutions 25 mL. Add it into a 50 mL conical flask, then add a certain amount of adsorbent, seal it with sealing film and place it at 22°C, 25°C and 31°C, respectively. The experimental data were used to fit the van Hoff formula, and the relevant thermodynamic parameters were obtained.

2.4. Adsorption diffusion model

The diffusion process of dye molecules in the adsorption process is divided into the following three steps: (1) dye molecules diffuse from the outside of the membrane; (2) the dye molecules reach the surface of the adsorbent; (3) dye molecules into the internal adsorbent adsorption. By fitting the diffusion model, we can understand the decision steps of controlling the diffusion rate of dye molecules. The diffusion model includes the diffusion equation outside the film and the diffusion equation of particles inside the film.

2.5. Orthogonal experimental design

The level of every single factor is obtained by adsorption experiment and design $L_9(3^4)$ orthogonal factor experiment. The four factors were initial dye solution concentration, reaction time, solution pH and adsorbent amount. The best experimental conditions of the adsorbent combination were determined through these four factors.

2.6. Desorption and regeneration test of adsorbent

MB was selected as the representative in this adsorption process, and 25 mg/L MB solution and 1.00 g adsorbent were added to a 50 mL conical flask. Until the adsorption is complete, separate the adsorbent, wash it repeatedly with distilled water and dry it for standby. Next, place the adsorbent in a closed glass container containing 100 mL distilled water as the regeneration solution, and place all glass containers in an ultrasonic oscillator containing water for 2 h. Finally, the oscillating adsorbent was collected, washed repeatedly with distilled water, and dried for the next adsorption–desorption experiment. The regeneration capacity of the adsorbent was assessed as a measure based on the removal ratio and adsorption capacity of MB in each experiment.

2.7. Formula

The formulas used in this paper are shown in Table 1.

3. Results and discussion

3.1. Material characterization

In-depth observation of the morphology of the adsorbent surface by SEM, the surface of BC-OA presents a porous structure similar to a 'honeycomb', and this may be due to the high temperature destroying its original structure, which is conducive to the formation of a denser and uniform pore structure. The porous structure can speed up the reaction rate to a certain extent [29]. According to the results of specific surface area and pore size distribution, the adsorption situation of the adsorbent can be predicted. Generally speaking, the larger the specific surface area, the richer the pore structure and the more adsorption sites provided, which is more conducive to the adsorption of dyes. Therefore, the specific surface area and pore size distribution are important characterization methods. The BET specific surface area of BC-OA is 442.26 m^2/g, and the total pore volume is 0.2101 mL/g. It can be seen that the BC-OA has a large specific surface area and rich pore structure.

The international IUPAC organisation classifies pores according to their size as micropores ($d < 2$ nm), mesopores (2 nm < d < 50 nm) and macropores ($d > 50$ nm). According to the measurement results, the pore size of BC-OA is mainly concentrated around 2 nm, and its average pore size d is 2.85 nm. Therefore, it can be inferred that most of the pore structure of BC-OA is microporous. This result corresponds to the nitrogen adsorption–desorption curve in the figure above. At the same time, the pore size of the adsorbent is closely related to the specific surface area. The more micropores, the larger the specific surface area. According to the pore size distribution diagram, it can be seen that BC-OA has a larger number of micropores and a larger corresponding specific surface area. The specific surface area of the agent corresponds to the result.

Fourier-transform infrared spectroscopy can be used to determine the existence of characteristic functional groups in the adsorbent. Observing the comparison of infrared spectra before and after adsorption makes it possible to qualitatively understand the functional groups that play a major role in the adsorption process. Fig. 1 compares the infrared spectra of the adsorbents before and after adsorption of MB. After being carbonized at high temperatures, the composition of the functional groups of BC-OA changed significantly. There is an obvious broad peak at the peak of 3,424.17 cm^{-1}, which is the hydroxylic (O–H) stretching vibration in the structure of alcohol and phenol associated with hydrogen bonding between molecules [30]. The absorption peak at 1,560.55 cm^{-1} is a characteristic peak of a benzene ring or aromatic, indicating that it contains benzene ring substances. The absorption peak at 1,154.71 cm^{-1} is generally considered the stretching vibration of the carbonyl group (C=O) in the structure of alcohol, phenol and ether [16]. The absorption peak at 873.69 cm^{-1} represents the stretching vibration of the ether bond (C–O–C) in the saturated six-membered dioxane ether [31]. These structures indicate that the high-temperature carbonization of bean dregs promotes the formation of aromatic groups. In other words, high-temperature carbonization is a process of aromatization. After BC-OA adsorbs MB, it can be seen from the spectrum that the peak of each corresponding functional group has an obvious 'red shift' phenomenon, which shows that the aromatic group participates in the entire adsorption process. This is because the π-electrons in the aromatic structure of BC-OA tend to have a strong electrostatic attraction to the cationic groups in MB, and the aromatic structure in BC-OA tends to form π–π conjugations with the aromatic ring groups in MB. However, when both of these effects are present, the effect of π–π conjugation is relatively weak. It conforms to the following adsorption

Table 1
Formula used in this article

	Name	Equations
Kinetic models used	Removal rate	$R = \frac{C_i - C_e}{C_i} \times 100\%$
	Equilibrium adsorption capacity	$q_e = \frac{(C_i - C_e)V}{m}$
	Pseudo-first-order	$\ln(q_e - q_t) = \ln q_e - k_1 t$
	Pseudo-second-order	$\frac{t}{q_t} = \frac{1}{k_2 q_e^2} + \frac{t}{q_e}$
	Intraparticle diffusion model	$q_t = k_{id} t^{1/2} + C$
	Extramembrane diffusion model	$\ln\left(1 - \frac{q_t}{q_e}\right) = -k_{fd} t$
Isotherm models used	Langmuir	$q_e = \frac{q_m K_L C_e}{1 + K_L C_e}$ $\frac{C_e}{q_e} = \frac{C_e}{q_m} + \frac{1}{K_L q_m}$ $R_L = \frac{1}{1 + K_L C_i}$
	Freundlich	$q_e = K_F C_e^{1/n}$ $\ln q_e = \frac{1}{n} \ln C_e + \ln K_F$
	Temkin	$q_e = a \ln K_T + a \ln C_e$
	Thermodynamics	$\Delta G° = -RT \ln K_d$ $\ln K_d = \frac{\Delta S°}{R} - \frac{\Delta H°}{RT}$

Notes: C_i and C_e are the initial concentration (mg/L) and equilibrium concentration (mg/L) of the dye solution, V is the volume of the dye solution (L), m is the mass of the adsorbent (g), q_t is the adsorption capacity at the time t (mg/g), k_1 is the first-order adsorption rate constant (min^{-1}), k_2 is the quasi-second-order adsorption rate constant (g/mg min), k_{id} is the diffusion rate constant (mg/g $min^{1/2}$), C is the constant (mg/g), k_{fd} is the liquid film diffusion coefficient (min^{-1}), q_m is the maximum adsorption capacity (mg/g), K_L is the Langmuir equilibrium constant (L/mg), K_F (L/g) and n are Freundlich constants respectively, K_T and a are Temkin constants, the value of K_T is related to the adsorption strength, K_d is the dispersion coefficient in the adsorption process, $\Delta S°$, $\Delta H°$ and $\Delta G°$ are entropy change (J/mol K), enthalpy change (J/mol) and Gibbs free energy change (J/mol), T is thermodynamic temperature (K) and R is ideal gas constant (8.314 J/mol K).

mechanism. The adsorption mechanism is mainly formed by electrostatic attraction and π–π interaction between the aromatic ring of the adsorbent and the aromatic structure of MB [32]. Therefore, the possible mechanism of BC-OA adsorption of MB dye is mainly reflected in electrostatic interaction and includes part of π–π conjugation.

After high-temperature carbonization of BC-OA, the diffraction angle 2θ appears at about 24.35°, which is the diffraction peak of graphite microcrystalline carbon d002 [33]. This shows that the cellulose structure is gradually transformed into microcrystalline carbon fiber after high-temperature treatment. The crystallinity is increased, which makes the BC-OA transform towards a more stable carbon compound, which is also the reason for the stable properties of BC. The value of the isoelectric point (pH_{pzc}) is closely related to the electrostatic force between the adsorbent and the adsorbate [34]. When the pH of the solution is less than pH_{pzc}, the surface of the adsorbent is positively charged; conversely, the surface of the adsorbent is negatively charged. According to Fig. 2, the isoelectric point of BC-OA is 8.6. According to experiments, the adsorption–desorption isotherm of BC-OA conforms to the type I adsorption isotherm, which is typical monolayer adsorption. Its characteristic is that the adsorption quickly reaches saturation, and the adsorption process of microporous materials is mostly expressed as the type I adsorption isotherm.

3.2. Adsorption kinetics

Adsorption kinetics is an important indicator for studying the practicality of adsorbents. Through the study of the kinetics of the reaction process, the description of the adsorption rate in the entire process can be used to adjust the design and specific parameters of the reactor [35]. The adsorption rate is the adsorption capacity of the adsorbent per unit time. As shown in Figs. 3 and 4, the removal ratio will gradually increase as the adsorption time increases. The adsorption reaction is mainly divided into three stages:

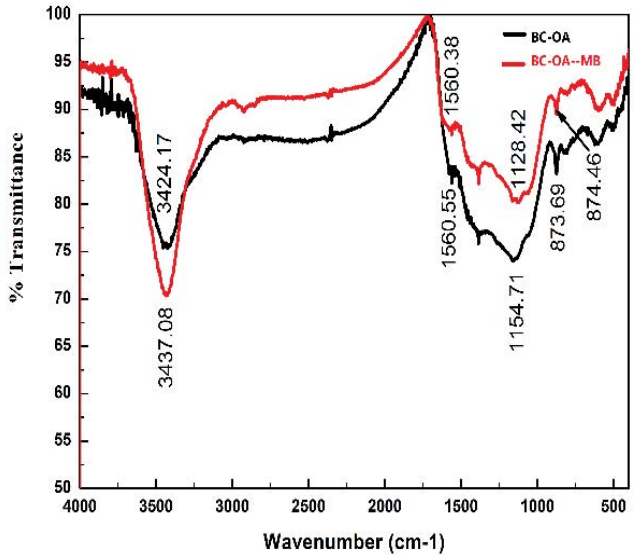

Fig. 1. Fourier-transform infrared spectra of BC-OA.

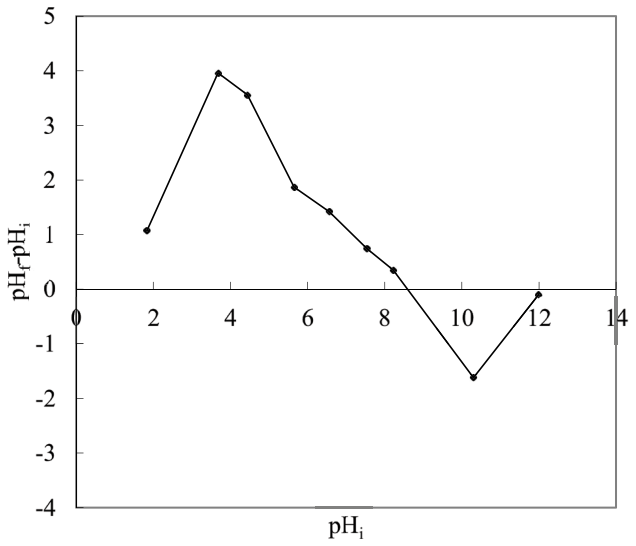

Fig. 2. The pH_{pzc} of BC-OA.

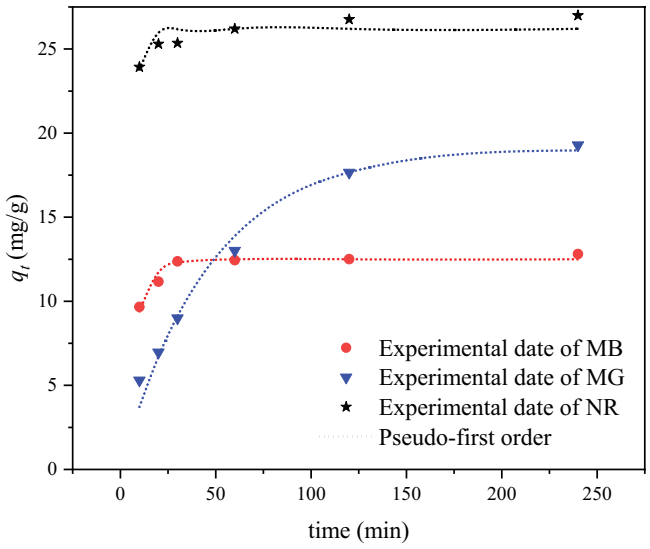

Fig. 3. Dynamical model fitting (pseudo-first-order).

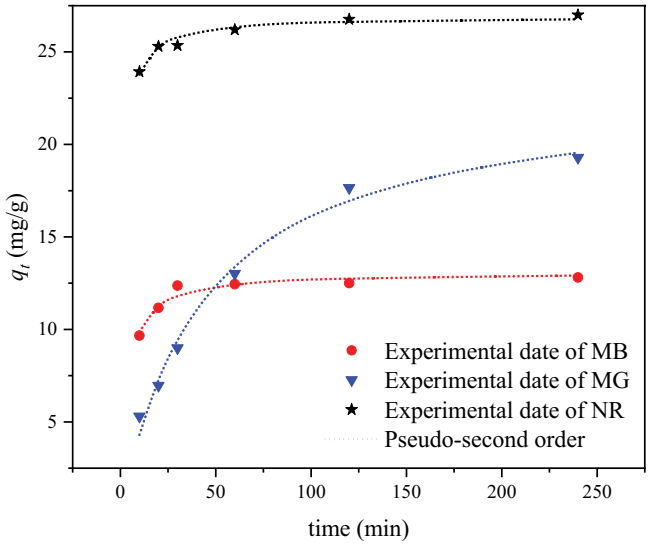

Fig. 4. Dynamical model fitting (pseudo-second-order).

the adsorption rate is very fast in the period of 0–30 min. In the time of 30–120 min, the reaction speed slowed down and the removal ratio increased slowly. When the reaction time reached 240 min, the adsorption reached equilibrium and the reaction rate was close to 0. Therefore, 2 h is selected as the best reaction time. On the one hand, all the adsorption reactions have reached an equilibrium state, and on the other hand, it saves time and increases work efficiency. According to the above analysis results, the removal ratio increases with the increase of the reaction time, and the reaction rate changes from fast to slow. This is because in the early stage of the reaction, NR molecules are adsorbed on the surface of the adsorbent, and then gradually diffuse inwards, the resistance of internal diffusion is relatively large, and the driving force of diffusion is weakened due to the decrease of external NR concentration. The combined effects of these two aspects make the reaction reach an equilibrium state [36]. The adsorption speed of adsorbents made of mostly residual biomass (OA-BC) is very fast, and the time required to reach equilibrium is also very short, which is of great significance in practical application.

The kinetic adsorption data can be fitted with the adsorption kinetic model. This study selected the pseudo-first-order kinetic model and the pseudo-second-order kinetic model proposed by Lagergren. Two kinetic models were used to fit the adsorption conditions of MB at different reaction times. The results are shown in Figs. 3 and 4, respectively. At the same time, the relevant parameters of the kinetic model are shown in Table 2. It can be seen that the R^2 value of the pseudo-first-order kinetic model is in the range of 0.6736–0.9341, the R^2 value of the pseudo-second-order kinetic model is in the range of 0.9396–0.9889, and the R^2 value is very high. However, according to $q_{e,cal}$ and $q_{e,exp}$,

Table 2
Related parameters table of kinetic models

Sample	Pseudo-first-order kinetic model			Pseudo-second-order kinetic model			
	k_1 (min^{-1})	$q_{e,cal}$ (mg/g)	R^2	k_2 (g/mg min)	$q_{e,cal}$ (mg/g)	R^2	$q_{e,exp}$ (mg/g)
MB	0.0139	12.4971	0.9341	0.0233	13.09	0.9396	12.90
MG	0.0217	19.077	0.9861	0.0009	23.114	0.9889	19.30
NR	0.2382	26.198	0.6736	0.0282	26.911	0.9536	27.10

the pseudo-second-order kinetic model is closer to the actual value, so the pseudo-second-order kinetic model is more suitable for the adsorption process, the adsorption process is dominated by chemical adsorption, and at the same time, it is also accompanied by part of the physical adsorption. In addition, the adsorption rate constant k is always less than 1.0000, indicating that the reaction process is very rapid [37].

3.3. Adsorption and diffusion model analysis

The diffusion process of dye molecules is divided into the following three steps: first, a liquid film is formed on the surface of the adsorbent due to hydration in the solution, and the dye molecules overcome the resistance of the liquid film to reach the surface of the adsorbent, also known as external diffusion; Second, dye molecules diffuse from the outer surface of the adsorbent to the inside, that is, internal diffusion; The third is the adsorption reaction of dye molecules on the active sites. The results show that the fitted curves for the intraparticle diffusion model do not cross the origin, indicating that internal diffusion is not the only factor controlling the rate of the adsorption reaction. Other factors may control the reaction rate, or other kinetic models may control it [38].

3.4. Effect of adsorbent dose

The effect of the amount of adsorbent added on MB, NR and MG adsorption effect is shown in Fig. 5. With the increase of the amount of adsorbent added, the removal ratio of MB gradually increased and reached an equilibrium state. The removal ratio increased from 31.26% to 48.65% for MB, and the corresponding adsorption capacity dropped from 1.72 to 0.43 mg/g. At the same time, according to the cross graph of removal ratio and adsorption capacity, and the best addition amount is 0.8 g/L, and the removal ratio is 43.76%. For NR, the removal ratio increased from 76.27% to 89.74%, and the effect of the addition amount was more obvious. The adsorption amount decreased from 47.67 to 18.70 mg/g, and the corresponding adsorption amount always showed a downward trend. For MG, the removal ratio increased from 53.36% to 81.88%, and the adsorption capacity decreased from 33.35 to 17.06 mg/g. According to the intersection of the removal ratio and the adsorption amount in the figure, the optimal amount of adsorbent added in the reaction process can be known. From the intersection of the three figures, it can be seen that the intersection area of the curve is concentrated at about 0.8, 0.4 and 0.4 g/L, respectively. However, considering that the raw material bean dregs for the preparation of adsorbents have a wide range of sources and are cheap and easy to obtain, the amount of adsorbent used in subsequent adsorption experiments is 0.8 g/L.

As the amount of adsorbent increases, the removal ratio gradually increases. The adsorbent provides enough adsorption sites for MB adsorption and increases the contact area. However, with the increase in the amount of adsorbent added, the number of adsorbent particles increased, and the adsorption surfaces overlapped, resulting in part of the adsorption sites being covered. Hence, the removal ratio reached an equilibrium state. The increase in the addition amount leads to a decrease in the corresponding unit adsorption amount [39]. Determining the influence of the amount of adsorbent addition on the adsorption effect is conducive to the rational use of resources. It avoids the effect of the adsorbent due to an insufficient amount of addition.

3.5. Effect of initial concentration of solution

According to the experimental determination of the effect of the concentrations of MB, NR and MG on the adsorption effect. When the concentration of MB, NR and MG is in the range of 25–250 mg/L, the removal ratio shows a downward trend. The removal ratio of BC-OA dropped from 43.76% to 12.32%, from 87.15% to 38.19%, and from 74.74% to 37.03%. It shows that the concentration of the solution has a significant effect on the removal effect of the adsorbent. The above results appear because the amount of adsorbent added is fixed, and the corresponding amount of adsorbed dye molecules is also limited. When the adsorbate concentration is low, the adsorption sites are more abundant, which is conducive to the binding of adsorbate molecules. However, when the concentration gradually increases, most of the limited adsorption sites are combined at this time, and the adsorbate molecules that can be adsorbed will decrease [40]. Therefore, even if the concentration of adsorbate in the solution gradually increases, the removal ratio also shows a downward trend. In addition, during the adsorption process, there is a significant repulsion between the adsorbent molecules already adsorbed and those subsequently adsorbed, which is not conducive to the adsorption process.

3.6. Effect of solution pH

The influence of the pH value of the solution on the adsorption effect is shown in Fig. 6. According to the figure, for MB, as the pH value of the solution increases, the removal ratio gradually rises, and the upward trend changes from fast to slow. The reason for this partial result may be that under acidic conditions, BC is present in solution as

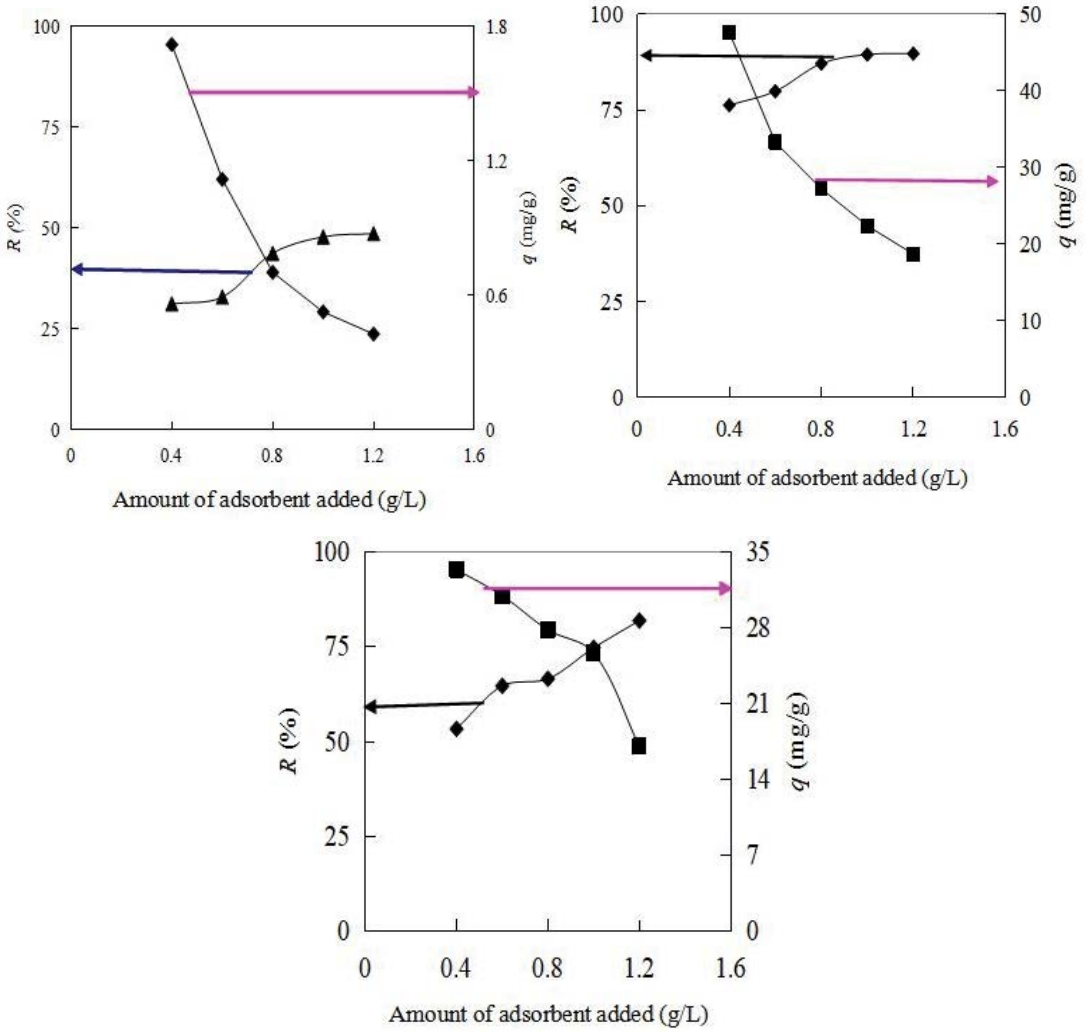

Fig. 5. Effect of adsorbent dosage on removal efficiency (a) MB, (b) NR and (c) MG).

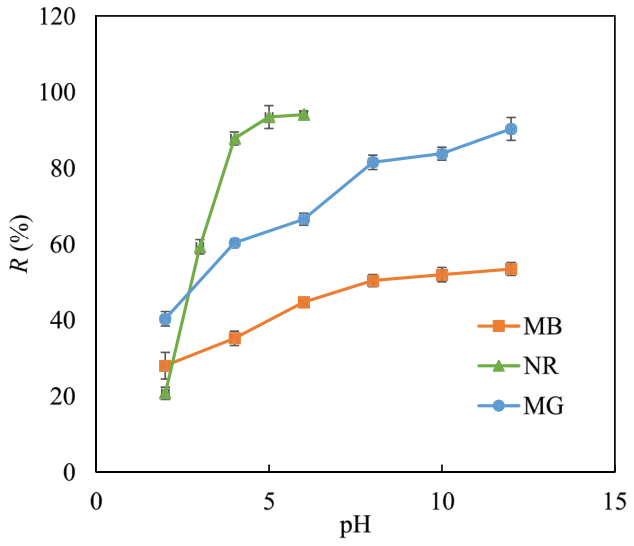

Fig. 6. Effect of pH value on removal efficiency.

protonated, whereas, in alkaline environments, it is present in the deprotonated form. Therefore, when the pH value of the solution is low, the active groups (such as hydroxylic groups) on the surface of BC-OA will be protonated due to the binding of H^+, competing with MB, which is also a cationic dye, for adsorption sites, so that effective adsorption sites will be cover. At the same time, H^+ and H_3O^+ ions will also compete with MB. With the gradual increase of the pH value of the solution, the competition for adsorption sites is weakened, and the protonation phenomenon also gradually weakens, transforming to deprotonation, the adsorption sites are released, and the removal ratio increases [41]. The results of this part are consistent with the results obtained from the previous infrared spectroscopy analysis. The electrostatic interaction is an important relationship in the entire adsorption process. According to the isoelectric point data, the isoelectric point of BC-OA is 8.6. When the pH of the solution > pH_{pzc}, the surface of the adsorbent carries a negative charge, which is conducive to the adsorption of MB; but when the pH of the solution is < pH_{pzc}, the positively charged adsorbent will prevent the adsorption of MB. Therefore,

according to the results in the above figure, the solution's pH value conditions suitable for the adsorbent's adsorption experiment are all greater than pH_{pzc}. This experimental result corresponds to the conclusion of the isoelectric point.

For NR, because NR will be converted into precipitation under alkaline conditions, when exploring the influence of solution pH on the adsorption effect, the pH values are set to 2.0–6.0 [42]. According to the figure, the removal ratio gradually increases with the increase of the pH value of the solution and finally reaches a steady state. When the pH value of the initial solution was 2.0, the removal ratio of BC-OA was 20.70%. When the pH value of the solution was 6.0, the corresponding removal ratio finally reached 94.03%. According to the data in Fig. 6, it can be seen that the pH value of the solution has a significant influence on the adsorption effect. When the pH value is higher, it is more conducive to adsorption. The above result is because neutral red ionizes cations in the solution. When the solution environment is strongly acidic, there is a lot of H^+, which will inhibit the dissociation of hydroxyl (O–H) and other functional groups from forming anions, and the corresponding electrostatic attraction will be weakened and the adsorption capacity will be weakened. However, when the pH value gradually increases, it is beneficial to the ionization of anions, making the reaction proceed in the direction beneficial to adsorption [43].

For MG, within the pH range of the experimental solution, the removal ratio of BC-OA increased from 40.30% to 90.27%, and the growth rate of the removal effect changed from fast to slow. According to the above experimental data, the upward trend of the graph is divided into two stages. When 2.0 < pH < 8.0, the H^+ concentration in the solution gradually decreases, and the chromogenic group of the MG dye molecule in the solution is a cation, which will compete with the H^+ in the solution. Therefore, when the H^+ concentration gradually decreases, the electrostatic attraction will facilitate the adsorption of the adsorbent. At this time, the removal ratio of BC-OA is 81.47%. However, when 8.0 < pH < 12.0, the growth of the removal ratio gradually slows down, indicating that the adsorbed MG molecules in the adsorbent and the free MG molecules in the solution have a repulsive reaction, which will 'neutralize' part of the electrostatic attraction, making the rise of adsorption slow. Therefore, the optimal pH of the MG adsorption experiment can be selected at about 8.0. The results are consistent with those obtained by infrared spectroscopy, which indicates that electrostatic attraction–repulsion is very important in dye adsorption experiments.

3.7. Effect of salt ion concentration in solution

During dyeing operations, large amounts of salt are usually added to promote the dyeing effect, so the presence of some salt ions in the actual dyeing wastewater makes it of practical importance to study the effect of salt ion concentration in solution adsorption effect [44]. According to the experimental results, the salt ion concentration has a significant impact on adsorption effect. For MB, when NaCl addition is less than 0.8 mol/L, the removal ratio drops sharply. The removal ratio of MB decreased from 43.76% to 30.73%, NR from 87.15% to 21.77%, MG from 74.74% to 40.45%, respectively. When the concentration of salt ions in the solution is low, salt ions will compete with dye molecules in ion exchange, shielding the electrostatic interaction between dye molecules and adsorbent so that the adsorption effect is weak. However, when the addition amount of NaCl gradually increased and was in the range of 0.8 to 4.0 mol/L, the removal ratio showed a trend of slow rise and finally showed a stable state. The removal ratio of MB gradually increased and finally reached 70.32%, NR 85.88% and MG 55.05%. When the concentration of salt ions in the solution increases, the number of pine ions and cations in the solution also increases accordingly, which makes the electrical double-layer structure formed by static interaction, thereby increasing the probability of the surface contact between the dye molecule and the suction agent, and the increased adsorption effect. At the same time, the concentration of salt ions increases, and the dye diameter structure forms, which is developing in the direction of adsorption [45]. However, within the range of NaCl addition in the experiment, the final removal ratio was lower than that without NaCl addition.

3.8. Orthogonal experiment analysis

In order to further seek the optimal combination of experimental conditions for the adsorption experiment, the influence degree of every single factor was determined according to the above experimental results. The $L_9(3^4)$ orthogonal factor levels designed by MB, NR and MG are Table 3. According to the above table, the orthogonal experiment was carried out, and the experimental results were sorted into the orthogonal experiment scheme and result table, and the orthogonal experiment scheme and result table of MB, NR and MG were Tables 4–6. According to the value of the comparison range *R*, the influence degree of the four single factors on MB is in the order of initial concentration of MB solution > pH > BC-OA addition > reaction time. The optimal experimental combination is MB solution concentration of 25 mg/L, BC-OA addition 1.0 g/L, reaction time 10 min, and solution pH 10.0. For NR, the optimal experimental combination is NR solution concentration of 25 mg/L, BC-OA dosage of 1.0 g/L, reaction time 60 min, and solution pH 6.0. For MG, the influence degree of the four factors was as follows: solution pH > addition level of BC-OA > reaction time > initial concentration of MG solution. The optimal experimental conditions were: MG solution concentration of 25 mg/L, an addition level of BC-OA 1.0 g/L, the reaction time of 60 min, and solution pH 8.0.

3.9. Adsorption isotherm

When experimental errors exist, the error distortion generated by linearized fitting may lead to misleading results. Fig. 7 and Table 7 show the results of nonlinear fits to three isotherm equations, including the Langmuir model, Freundlich model, and Temkin model. It was found that the adsorption of MB, NR and MG by BC gradually increased with the increase of initial concentration. This increasing trend is more obvious in the first 30 min of the reaction process. Beyond this range, the adsorption capacity of BC to three dyes tends to be flat. In all three models,

Table 3
Adsorbed dye orthogonal factor analysis data sheet

Adsorbent	Level	Experimental factors			
		Initial concentration (mg/L) *A*	Addition amount of adsorbent (g/L) *B*	Time (min) *C*	Solution pH *D*
	1	25	0.6	10	4.0(6.0)
MB	2	50	0.8	30	6.0(8.0)
	3	100	1	60	8.0(10.0)
	1	25	0.6	10	4.0
NR	2	50	0.8	30	5.0
	3	100	1	60	6.0
	1	25	0.8	10	6.0
MG	2	50	1	30	8.0
	3	100	1.2	60	10.0

Table 4
Orthogonal experiment scheme and results table of MB

Experiment number	MB initial concentration (mg/L) *A*	BC-OA addition amount (g/L) *B*	Time (min) *C*	Solution pH *D*	Removal rate (%)
1	25	0.6	10	10.0	46.35
2	25	0.8	30	6.0	42.31
3	25	1.0	60	8.0	41.18
4	50	0.6	30	8.0	32.94
5	50	0.8	60	10.0	40.58
6	50	1.0	10	6.0	40.87
7	100	0.6	60	6.0	22.29
8	100	0.8	10	8.0	33.10
9	100	1.0	30	10.0	37.62
K_1	129.84	101.58	120.32	105.47	
K_2	114.39	115.98	112.87	107.22	
K_3	93.01	119.67	104.04	124.55	
k_1	43.28	33.86	40.11	35.16	
k_2	38.13	38.66	37.62	35.74	
k_3	31.00	39.89	34.68	41.52	
Range	12.28	6.03	5.42	6.36	
Primary and secondary order	*A* > *D* > *B* > *C*				
Optimal levels	*A*1	*B*3	*C*1	*D*3	
Optimal combination	*A*1*B*3*C*1*D*3				

the sorption of MB, NR and MG by BC-OA had the highest R^2 values in the Langmuir model, with R^2 values of 0.9565, 0.9811 and 0.9825, respectively. It was shown that the MB and MG adsorption processes were monolayer adsorption and the q_m obtained were 294.04, 583.50 and 1,058.36 mg/g, respectively. The separation factors (R_L) of the Langmuir model all remained between 0 and 1, which is favourable adsorption (preferential adsorption), indicating that the adsorption process is favourable. Moreover, the linear correlation coefficients R^2 of Freundlich models for MB, NR and MG were 0.9429, 0.9811 and 0.9685, respectively. It is assumed that the adsorption of MB, NR and MG on the surface of BC-OA exists as non-homogeneous surface adsorption and is not limited to monolayer adsorption. K_F (L/mg) is a constant related to the capacity of BC; n is a constant related to the fixation intensity of BC in the equation. The parameters K_F obtained by Freundlich were 1.455, 5.079, and 3.222 L/mg with parameters n of 1.39, 1.52, and 1.29, respectively (n > 1 for preferential adsorption). The values exhibited by both K_F and n indicate that the adsorbent is effective in adsorption. In addition, the R^2 values of the correlation coefficients for the Temkin isotherm fit were 0.8838, 0.9420

Table 5
Orthogonal experiment scheme and results table of NR

Experiment number	NR initial concentration (mg/L) *A*	BC-OA addition amount (g/L) *B*	Time (min) *C*	Solution pH *D*	Removal rate (%)
1	25	0.6	10	6.0	75.79
2	25	0.8	30	4.0	73.82
3	25	1.0	60	5.0	92.29
4	50	0.6	30	5.0	66.42
5	50	0.8	60	6.0	90.18
6	50	1.0	10	4.0	67.82
7	100	0.6	60	4.0	55.28
8	100	0.8	10	5.0	57.18
9	100	1.0	30	6.0	84.61
K_1	241.90	197.48	200.79	196.92	
K_2	224.42	221.19	224.85	215.90	
K_3	197.07	244.72	237.75	250.58	
k_1	80.63	65.83	66.93	65.64	
k_2	74.81	73.73	74.95	71.97	
k_3	65.69	81.57	79.25	83.53	
Primary and secondary order	*D* > *B* > *A* > *C*				
Optimal levels	*A*1	*B*3	*C*3	*D*3	
Optimal combination	*A*1*B*3*C*3*D*3				

Table 6
Orthogonal experiment scheme and results table of MG

Experiment number	MG initial concentration (mg/L) *A*	BC-OA addition amount (g/L) *B*	Time (min) *C*	Solution pH *D*	Removal rate (%)
1	25	0.8	10	10.0	24.98
2	25	1.0	30	6.0	29.51
3	25	1.2	60	8.0	61.26
4	50	0.8	30	8.0	13.31
5	50	1.0	60	10.0	37.09
6	50	1.2	10	6.0	10.32
7	100	0.8	60	6.0	22.89
8	100	1.0	10	8.0	57.12
9	100	1.2	30	10.0	25.38
K_1	115.75	61.18	92.42	62.73	
K_2	60.73	123.73	68.21	131.70	
K_3	105.40	96.97	121.25	87.45	
k_1	38.58	20.39	30.81	20.91	
k_2	30.36	41.24	22.74	43.90	
k_3	35.13	32.32	40.42	29.15	
Range	8.22	20.85	17.68	22.99	
Primary and secondary order	*D* > *B* > *C* > *A*				
Optimal levels	*A*1	*B*2	*C*3	*D*2	
Optimal combination	*A*1*B*2*C*3*D*2				

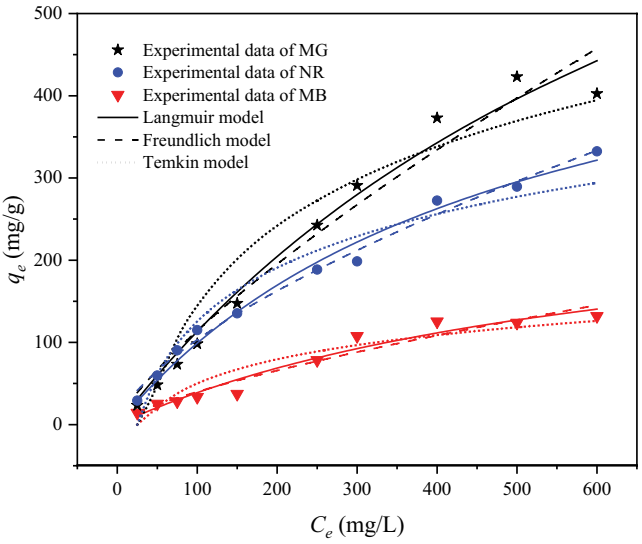

Fig. 7. Fitting isotherm curves for the adsorption of three dyes by BC-OA.

and 0.9231, respectively, indicating that the adsorption process is affected by temperature to some extent. The model is general and applicable to a wide range of applications.

3.10. Adsorption thermodynamics

The analysis of the thermodynamics of the adsorption reaction provides insight into the variation of the thermal energy during the reaction and the spontaneity of the adsorption process. The thermodynamic parameters of adsorption, including the enthalpy change ($\Delta H°$), entropy change ($\Delta S°$) and Gibbs free energy change ($\Delta G°$), as derived from the thermodynamics equations in Table 8. The positive and negative values, as well as the magnitude, give an idea of the nature of the adsorption reaction. At the experimentally set temperatures of 22°C, 25°C and 31°C (corresponding to 295, 298 and 304 K, respectively), the thermodynamic parameters obtained are collated as shown in Table 8.

As can be seen from the data in the table, $\Delta G°$ is always less than 0 at different temperatures, which indicates that the process is spontaneous for all three dyes adsorbed. As the temperature increased from 295 to 304 K, the $\Delta G°$ values were –0.98, –1.13, –1.53 kJ/mol for MB, –3.96, –4.08, –4.22 kJ/mol for NR, –3.69 kJ/mol for MG, –3.89, –4.08 kJ/mol, respectively. As the temperature increases, the reaction's spontaneity becomes greater, and the adsorption of MB, NR and MG by BC-OA is a spontaneous reaction process. Further evidence that the reaction is heat-absorbing is based on the $\Delta H°$ values of 7.12, 8.13 and 1.039 kJ/mol for MB and NR and MG, respectively, which are all positive values. At the temperature of 303K, $\Delta H°$ was 7.74 kJ/mol, $\Delta G°$ was –10.26 kJ/mol, which was an endothermic spontaneous reaction [46]. The study using graphene to adsorb MB found that temperature increase is conducive to the reaction, and the same results were obtained [47].

In addition, the value of $\Delta S°$ represents the disorderly nature of the reaction system. $\Delta S°$ values of 56.66 and 5.025 J/mol K for MB and MG indicate an increase in disorder during the adsorption of MB and MG molecules by the adsorbent in the adsorption reaction. For NR, the $\Delta S°$ value of –24.32 J/mol K is negative, unlike MB and MG, indicating that the reaction becomes less chaotic in the system during the adsorption process.

When the adsorption process of the three dyestuffs was confirmed to be spontaneous, this indicates that this type of adsorption can occur on its own without external assistance. This increases the possibility of its application to the treatment of actual dye wastewater. The heat-absorbing reaction indicates that the adsorption reaction proceeds positively at elevated temperatures, which is a good guide for controlling the reaction rate in practical applications.

3.11. Regeneration adsorption experiment

According to the experimental method in 2.6, the regeneration adsorption experiment of BC-OA for 5 cycles of adsorption–desorption was carried out, and the experimental data of adsorption on MB were sorted out. The Recovery ranged from 42.22% to 43.76%, and the q_e ranged from 12.19 to 12.90 mg/g. Recovery represents the regeneration efficiency (%) during the adsorbent cycle, and q_e represents the adsorption capacity (mg/g) during the cycle. For BC-OA, the adsorbed dye MB is almost completely desorbed and can be used for the next adsorption, which shows that ultrasonic treatment of BC-OA does not destroy its morphological structure, which also confirms the stable structure of BC.

3.12. Adsorption mechanism

It is of practical significance to study the adsorption mechanism and law of dye molecules by adsorbent to evaluate its application and environmental impact. At present, studies have shown that the common adsorption mechanisms include electrostatic interaction, π–π conjugation, hydrogen bonding, intermolecular force [48]. This study explored the adsorption mechanism by analyzing the results of the characterization determination and experimental

Table 7
Parameters related to the fitting of each isotherm

Sample	Langmuir isotherm			Freundlich isotherm				Temkin isotherm		
	q_m (mg/g)	K_L (L/mg)	R_L	R^2	K_F (L/mg)	n	R^2	K_T	a	R^2
MB	294.04	0.0015	0.00–0.96	0.9565	1.455	1.39	0.9429	0.032	42.46	0.8838
NR	583.50	0.0020	0.45–0.95	0.9870	5.079	1.52	0.9811	0.038	94.18	0.9420
MG	1058.36	0.0012	0.58–0.97	0.9825	3.222	1.29	0.9685	0.028	139.55	0.9231

Table 8
Related parameters table of thermodynamics (temperatures of 295, 298 and 304 K)

Sample	T (K)	K_d	$\Delta H°$ (kJ/mol)	$\Delta S°$ (J/mol K)	$\Delta G°$ (kJ/mol)
	295	1.4708			–0.98
MB	298	1.5754	7.12	56.66	–1.13
	304	1.8682			–1.53
	295	5.0341			–3.96
NR	298	5.1898	8.13	–24.32	–4.08
	304	5.2772			–4.22
	295	4.5082			–3.69
MG	298	4.7986	1.039	5.025	–3.89
	304	5.0136			–4.08

adsorption. High-temperature carbonization made the surface of adsorbent BC-OA present a 'honeycomb' structure, enhanced the degree of aromatization, and greatly changed the number and type of surface functional groups. The rich microporous composition and surface functional groups of BC-OA play an important role in adsorption. High-temperature carbonization is beneficial to the formation of pores on the surface of carbon but accelerates the decomposition of functional groups. BC-OA makes the specific surface area increase because of its abundant pore structure, but not specific surface area, and the key factors that decide adsorption, BC-OA's main role for chemical adsorption in the process of adsorption reaction is mainly manifested in the following two aspects: on the one hand, the BC-OA π electrons in the aromatic ring structure with cationic groups of adsorbate N^+ strong electrostatic attraction; On the other hand, π–π conjugation exists between π electrons in the aromatic ring structure of BC-OA and π electrons in the benzene ring of the adsorbent, but the π–π conjugation effect is much weaker than that of electrostatic attraction.

Therefore, the adsorption process of BC-OA can be divided into the following three stages. First, adsorbent molecules can enter the porous channels of BC-OA and then be adsorbed to negatively charged positions on the surface by electrostatic attraction. With the increase of adsorbent concentration, cations migrate to the diffusion layer. Finally, the π electrons in the aromatic ring structure of BC-OA form a specific chemical interaction relationship with the cationic groups N^+ and π electrons in the aromatic ring structure of the adsorbent. In addition to the direct electrostatic interaction between oxygen atoms in oxygen-containing functional groups and MB, the six-membered ring π electrons formed by the sp^2 hybridization of graphene carbon atoms also have π–π conjugation with the π electrons in the benzene ring in MB [49]. The adsorption of MB by soybean BC prepared by the hydrothermal method was found to be in accordance with the pseudo-second-order model, indicating that there is a chemical force in the adsorption process, that is, the interaction between the delocalized π electrons on the surface of the adsorbent, the N^+ of cationic dye and the π electrons in benzene ring [50]. Some studies have used activated sludge to prepare BC. Sludge BC is alkaline and contains oxygen-containing functional groups and inorganic mineral components on the surface. According to the analysis of experimental results, it is found that the mechanism of interaction with MB solution includes electrostatic action, π–π conjugation and nitrogen and phosphorus interaction [51].

4. Conclusions

In this paper, BC was prepared using okara as the raw material. Combined with the characterisation, BC-OA was found to have more micropores and a larger corresponding specific surface area, where the specific surface area was 442.26 m^2/g. The high-temperature carbonisation promotes the formation of aromatic groups and also increases the crystallinity of BC-OA, making it more stable. BC-OA has a good adsorption capacity for dyes, especially MG. The maximum adsorption of MB, MG and NR by BC-OA was 294.04, 1,058.36 and 583.50 mg/g, respectively. The adsorption process of BC-OA was more in line with the pseudo-second-order, with the adsorption rate constant k always less than 1.0000. However, the fitted curve of the dye particle internal diffusion model did not cross the origin, indicating that other factors influenced the reaction rate in addition to internal diffusion. The results of the mechanistic analysis show that the adsorption process is unilamellar and easy to carry out and that the interactions are electrostatic and π–π conjugated. The π electrons in the BC-OA aromatic ring structure have a strong electrostatic attraction to the cationic group in the dye and a weak π–π conjugation between the π electrons and the benzene electrons in the dye. The adsorption process was heated, which was more favourable for the reaction. This paper investigates the use of food processing waste and working adsorbents. BC-OA was found to be a promising adsorbent for the treatment of dye wastewater because of its low preparation cost, fast fixation of pollutants and recyclability, in the hope of providing new ideas for the treatment of dye wastewater.

Acknowledgment

This work was supported by the Science and Technology Research Program of Chongqing Municipal Education Commission of China (Grant No. KJQN201901343) and the Science and Technology Research Program of Chongqing University of Arts and Sciences (Grant No. R2019FLX19 and P2021YL12).

References

[1] A. Patel, S. Soni, J. Mittal, A. Mittal, C. Arora, Sequestration of crystal violet from aqueous solution using ash of black turmeric rhizome, Desal. Water Treat., 220 (2021) 342–352.
[2] K. Kosek, A. Luczkiewicz, S. Fudala-Książek, K. Jankowska, M. Szopińska, O. Svahn, J. Tränckner, A. Kaiser, V. Langas, E. Björklund, Implementation of advanced micropollutants removal technologies in wastewater treatment plants (WWTPS) – examples and challenges based on selected EU countries, Environ. Sci. Policy, 112 (2020) 213–226.
[3] H. Chen, X. Yu, X. Wang, Y. He, C. Zhang, G. Xue, Z. Liu, H. Lao, H. Song, W. Chen, Y. Qian, A. Zhang, X. Li, Dyeing and finishing wastewater treatment in China: state of the art and perspective, J. Cleaner Prod., 326 (2021) 129353, doi: 10.1016/j.jclepro.2021.129353.

[4] S. Mishra, L. Cheng, A. Maiti, The utilization of agro-biomass/byproducts for effective bio-removal of dyes from dyeing wastewater: a comprehensive review, J. Environ. Chem. Eng., 9 (2021) 104901, doi: 10.1016/j.jece.2020.104901.
[5] C. Arora, P. Kumar, S. Soni, J. Mittal, A. Mittal, B. Singh, Efficient removal of malachite green dye from aqueous solution using *Curcuma caesia* based activated carbon, Desal. Water Treat., 195 (2020) 341–352.
[6] J. Mittal, Permissible synthetic food dyes in India, Resonance, 25 (2020) 567–577.
[7] A. Mariyam, J. Mittal, F. Sakina, R.T. Baker, A.K. Sharma, A. Mittal, Efficient batch and fixed-bed sequestration of a basic dye using a novel variant of ordered mesoporous carbon as adsorbent, Arabian J. Chem., 14 (2021) 103186, doi: 10.1016/j.arabjc.2021.103186.
[8] Mu. Naushad, A.A. Alqadami, Z.A. AlOthman, I.H. Alsohaimi, M.S. Algamdi, A.M. Aldawsari, adsorption kinetics, isotherm and reusability studies for the removal of cationic dye from aqueous medium using arginine modified activated carbon, J. Mol. Liq., 293 (2019) 111442, doi: 10.1016/j.molliq.2019.111442.
[9] F.P. de Freitas, A.M.M.L. Carvalho, A. de Cássia Oliveira Carneiro, M.A. de Magalhães, M.F. Xisto, W.D. Canal, Adsorption of neutral red dye by chitosan and activated carbon composite films, Heliyon, 7 (2021) e07629, doi: 10.1016/j.heliyon.2021.e07629.
[10] M. Iram, C. Guo, Y. Guan, A. Ishfaq, H. Liu, Adsorption and magnetic removal of neutral red dye from aqueous solution using Fe_3O_4 hollow nanospheres, J. Hazard. Mater., 181 (2010) 1039–1050.
[11] A. Mohamed, M. Ghobara, M. Abdelmaksoud, G. Mohamed, A novel and highly efficient photocatalytic degradation of malachite green dye via surface modified polyacrylonitrile nanofibers/biogenic silica composite nanofibers, Sep. Purif. Technol., 210 (2019) 935–942.
[12] J. Mittal, Permissible synthetic food dyes in India, Resonance, 25 (2020) 567–577.
[13] A. Gupta, C. Balomajumder, Simultaneous removal of Cr(VI) and phenol from binary solution using *Bacillus* sp. immobilized onto tea waste biomass, J. Water Process Eng., 6 (2015) 1–10.
[14] Y. Wang, Y. Liu, K. Wang, S. Song, P. Tsiakaras, H. Liu, Preparation and characterization of a novel KOH activated graphite felt cathode for the electro-Fenton process, Appl. Catal., B, 165 (2015) 360–368.
[15] J. Zhao, Y. Dai, Tetracycline adsorption mechanisms by NaOH-modified biochar derived from waste *Auricularia auricula* dregs, Environ. Sci. Pollut. Res., 29 (2022) 9142–9152.
[16] F. Wang, H. Sun, X. Ren, Y. Liu, H. Zhu, P. Zhang, C. Ren, Effects of humic acid and heavy metals on the sorption of polar and a polar organic pollutants onto biochars, Environ. Pollut., 231 (2017) 229–236.
[17] Y.J. Dai, K.X. Zhang, X.B. Meng, J.J. Li, X.T. Guan, Q.Y. Sun, Y. Sun, W.S. Wang, M. Lin, M. Liu, S.S. Yang, Y.J. Chen, F. Gao, X. Zhang, Z.H. Liu, New use for spent coffee ground as an adsorbent for tetracycline removal in water, Chemosphere, 215 (2019) 163–172.
[18] S.N. Surip, A.S. Abdulhameed, Z.N. Garba, S.S.A. Syed-Hassan, K. Ismail, A.H. Jawad, H_2SO_4-treated Malaysian low rank coal for methylene blue dye decolourization and COD reduction: optimization of adsorption and mechanism study, Surf. Interfaces, 21 (2020) 100641, doi: 10.1016/j.surfin.2020.100641.
[19] L. Liu, W. Fang, M. Yuan, X. Li, X. Wang, Y. Dai, Metolachlor-adsorption on the walnut shell biochar modified by the fulvic acid and citric acid in water, J. Environ. Chem. Eng., 9 (2021) 106238, doi: 10.1016/j.jece.2021.106238.
[20] B. Kayan, D. Kalderis, E. Kulaksız, B. Gözmen, Adsorption of malachite green on Fe-modified biochar: influencing factors and process optimization, Desal. Water Treat., 74 (2017) 383–394.
[21] L. Liu, X. Wang, W. Fang, X. Li, D. Shan, Y. Dai, Adsorption of metolachlor by a novel magnetic illite–biochar and recovery from soil, Environ. Res., 204 (2022) 111919, doi: 10.1016/j.envres.2021.111919.
[22] M. Rajabi, B. Mirza, K. Mahanpoor, M. Mirjalili, F. Najafi, O. Moradi, H. Sadegh, R. Shahryari-Ghoshekandi, M. Asif, I. Tyagi, S. Agarwal, V. Gupta, Adsorption of malachite green from aqueous solution by carboxylate group functionalized multi-walled carbon nanotubes: determination of equilibrium and kinetics parameters, J. Ind. Eng. Chem., 34 (2016) 130–138.
[23] L. Liu, X. Li, X. Wang, Y. Wang, Z. Shao, X. Liu, D. Shan, Z. Liu, Y.J. Dai, Metolachlor adsorption using walnut shell biochar modified by soil minerals, Environ. Pollut., 308 (2022) 119610.
[24] Z. Liu, S. Cui, L. Zhang, Z. Zhang, R. Hough, Q. Fu, Y.-F. Li, L. An, M. Huang, K. Li, Y. Ke, F. Zhang, Occurrence, variations, and risk assessment of neonicotinoid insecticides in Harbin section of the Songhua River, northeast China, Environ. Sci. Ecotechnol., 8 (2021) 100128, doi: 10.1016/j.ese.2021.100128.
[25] J.H. Qu, X. Tian, X.B. Zhang, J.Y. Yao, J.Q. Xue, K.G. Li, B. Zhang, L. Wang, Y. Zhang, Free radicals-triggered reductive and oxidative degradation of highly chlorinated compounds via regulation of heat-activated persulfate by low-molecular-weight organic acids, Appl. Catal., B, 310 (2022) 121359, doi: 10.1016/j.apcatb.2022.121359.
[26] J. Liu, J. Zhou, Z.H. Wu, X. Tian, X.Y. An, Y. Zhang, G.S. Zhang, F.X. Deng, X.L. Meng, J.H. Qu, Concurrent elimination and stepwise recovery of Pb(II) and bisphenol A from water using β–cyclodextrin modified magnetic cellulose: adsorption performance and mechanism investigation, J. Hazard. Mater., 432 (2022) 128758, doi: 10.1016/j.jhazmat.2022.128758.
[27] Y. Liu, S. Cui, Y. Ma, Q. Jiang, X. Zhao, Q. Cheng, L. Guo, H. Jia, L. Lin. Brominated flame retardants (BFRs) in marine food webs from Bohai Sea, China, Sci. Total Environ., 772 (2021) 145036, doi: 10.1016/j.scitotenv.2021.145036.
[28] J.H. Qu, J.J. Shi, Y.H. Wang, H. Tong, Y.J. Zhu, L.S. Xu, Y.F. Wang, B. Zhang, Y. Tao, X. Dai, H. Zhang, Y. Zhang, Applications of functionalized magnetic biochar in environmental remediation: a review, J. Hazard. Mater., 434 (2022) 128841, doi: 10.1016/j.jhazmat.2022.128841.
[29] S. Li, Y. Xu, X. Jing, G. Yilmaz, D. Li, L. Turng, Effect of carbonization temperature on mechanical properties and biocompatibility of biochar/ultra-high molecular weight polyethylene composites, Composites, Part B, 196 (2020) 108120, doi: 10.1016/j.compositesb.2020.108120.
[30] L. Liu, Y.J. Dai, Strong adsorption of metolachlor by biochar prepared from walnut shells in water, Environ. Sci. Pollut. Res., 28 (2021) 48379–48391.
[31] Q. Zheng, Y. Wang, Y. Sun, H. Niu, J. Zhou, Z. Wang, J. Zhao, FTIR study on the structural properties of biochar prepared from different materials and carbonization methods, Spectrosc. Spectral Anal., 34 (2014) 962–966.
[32] X. Ji, L. Lv, F. Chen, C. Yang, Sorption business and mechanisms of organic dyes by straw biochar, Acta Sci. Circum., 36 (2016) 1648–1654.
[33] J. Zhao, F. Gao, Y. Sun, W. Fang, X. Li, Y. Dai, New use for biochar derived from bovine manure for tetracycline removal, J. Environ. Chem. Eng., 9 (2021) 105585, doi: 10.1016/j.jece.2021.105585.
[34] J. Lützenkirchen, A. Abdelmonem, R. Weerasooriya, F. Heberling, V. Metz, R. Marsac, Adsorption of dissolved aluminum on sapphire-c and kaolinite: implications for points of zero charge of clay minerals, Geochem. Trans., 15 (2014) 1–14.
[35] Y. Ji, Q. Wu, J. Zhou, W. Zhuang, H. Ying, Adsorption equilibrium, kinetic and dynamic adsorption of vanillin onto macroporous resin, Chin. J. Bioprocess Eng., 16 (2018) 16–22.
[36] Y. Ke, S. Cui, Q. Fu, R. Hough, Z. Zhang, Y.-F. Li, Effects of pyrolysis temperature and aging treatment on the adsorption of Cd^{2+} and Zn^{2+} by coffee grounds biochar, Chemosphere, 296 (2022) 134051, doi: 10.1016/j.chemosphere.2022.134051.
[37] J. Cheng, H. Wang, D. Zhou, Adsorption and desorption of Cu^{2+} and Cd^{2+} on the surface of modified nano black carbon, Res. Environ. Sci., 24 (2011) 1409–1415.
[38] L. Eskandarian, M. Arami, E. Pajootan. Evaluation of adsorption characteristics of multi-walled carbon nanotubes modified by a

poly(propylene imine) dendrimer in single and multiple dye solutions: isotherms, kinetics, and thermodynamics, J. Chem. Eng. Data, 59 (2014) 444–454.
[39] Q. Yue, W. Wang, B. Gao, X. Xu, J. Zhang, L. Qian, Phosphate removal from aqueous solutions by adsorption on modified giant reed, Water Environ. Res., 82 (2010) 374–381.
[40] M. Sajab, C. Chia, S. Zakaria, P. Khiew, Cationic and anionic modifications of oil palm empty fruit bunch fibers for the removal of dyes from aqueous solutions, Bioresour. Technol., 128 (2013) 571–577.
[41] Y. Xia, T. Li, J. Chen, C. Cai, Polyaniline (skin)/polyamide 6 (core) composite fiber: preparation, characterization and application as a dye adsorbent, Synth. Metals, 175 (2013) 163–169.
[42] J. Wang, T. Feng, Y. Hu, R. Tang, Study on the adsorption property of corncob powder for neutral red, Chem. Bull., 79 (2016) 981–985.
[43] X. Li, Y. Song, M. Jia, F. Wang, Y. Bian, X. Jiang, Research progress on adsorption and mechanism of organic pollutants by biomass charcoal, Acta Pedologica Sinic, 54 (2017) 1313–1325.
[44] U. Guyo, Application of response surface methodology for Cd(II) adsorption on maize tassel-magnetite nanohybrid adsorbent, J. Environ. Chem. Eng., 3 (2015) 2472–2483.
[45] Z. Wu, H. Liu, H. Zhang, Research progress on mechanism of influence of ionic strength on adsorption, Environ. Chem., 29 (2010) 997–1003.
[46] L. Fan, C. Luo, M. Sun, X. Li, H. Qiu, Highly selective adsorption of lead ions by water dispersible magnetic chitosan/graphene oxide composites, Colloids Surf., B, 103 (2013) 523–529.
[47] T. Wu, X. Cai, S. Tan, H. Li, J. Liu, W. Yang, Adsorption characteristics of acrylonitrile, p-toluenesulfonic acid, 1-naphthalenesulfonic acid and methyl blue on graphene in aqueous solutions, Chem. Eng. J., 173 (2011) 144–149.
[48] Y. Dai, J. Shi, N. Zhang, Z. Pan, C. Xing, X. Chen, Current research trends on microplastics pollution and impacts on agro-ecosystems: a short review, Sep. Sci. Technol., 57 (2022) 656–669.
[49] S. Yang, S. Chen, Y. Chang, A. Cao, Y. Liu, H. Wang, Removal of methylene blue from aqueous solution by graphene oxide, J. Colloid Interface Sci., 359 (2011) 24–29.
[50] B. Wang, Y. Zhai, T. Wang, S. Li, C. Peng, Z. Wang, C. Li, B. Xu, Fabrication of bean dreg-derived carbon with high adsorption for methylene blue: effect of hydrothermal pretreatment and pyrolysis process, Bioresour. Technol., 274 (2019) 525–537.
[51] S. Fan, Y. Wang, Z. Wang, J. Tang, J. Tang, X. Li, Removal of methylene blue from aqueous solution by sewage sludge-derived biochar: adsorption kinetics, equilibrium, thermodynamics and mechanism, J. Environ. Chem. Eng., 5 (2017) 601–611.